Plasmon Field-Enhanced Fluorescence Energy Transfer for Hairpin Aptamer Assay Readout

Khulan Sergelen,[†,‡,§] Stefan Fossati,[†] Aysegül Turupcu,[‖] Chris Oostenbrink,[‖] Bo Liedberg,[‡] Wolfgang Knoll,[†] and Jakub Dostálek*,[†]

[†]BioSensor Technologies, AIT-Austrian Institute of Technology, Muthgasse 11, 1190 Vienna, Austria

[‡]Nanyang Technological University, Centre for Biomimetic Sensor Science, School of Materials Science and Engineering, 50 Nanyang Drive, Singapore 637553

[§]International Graduate School on Bionanotechnology, University of Natural Resources and Life Sciences, Austrian Institute of Technology, and Nanyang Technological University, 1190 Vienna, Austria

[‖]University of Natural Resources and Life Sciences, Institute of Molecular Modeling and Simulation, Muthgasse 18, 1190 Vienna, Austria

⑤ *Supporting Information*

ABSTRACT: Surface plasmon field-enhanced fluorescence energy transfer is employed for sensitive optical readout of a reversible hairpin aptamer assay that is suitable for continuous monitoring of low-molecular-weight chemical analytes. A hairpin aptamer specific to adenosine and adenosine triphosphate with Alexa Fluor 647 fluorophore attached to its 5′ end was anchored via 3′ end thiol to a gold thin film. Molecular spacers were used to control the distance of the fluorophore from the surface in the aptamer "off" and "on" states. The specific binding of the target analyte changes the aptamer conformation, which alters the distance of the fluorophore from the gold surface and translates to variations in the detected fluorescence intensity. The plasmonically mediated fluorescence signal increases the measured signal-to-noise ratio and allows for real-time observation of the analyte binding. Theoretical as well as experimental study of the optical signal dependence on fluorophore orientation, design of spacers, and angular distribution of collected light is presented for rational design of the assay. The detected sensor signal increased by a factor as large as 23 upon switching the aptamer from the "off" to "on" state due to the hairpin opening associated with the specific capture of target analyte.

KEYWORDS: aptamer, surface plasmon field-enhanced fluorescence, plasmonic amplification, quenching, adenosine triphosphate, fluorescence energy transfer
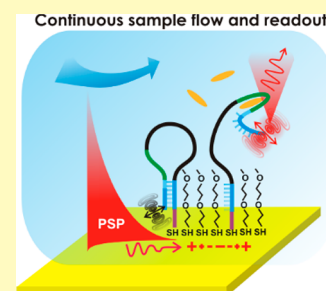
The coupling of fluorophores with the confined field of surface plasmons originating from collective oscillations of the electron density at metallic surfaces offers powerful means for the amplification of emitted fluorescence light intensity.[1,2] The plasmonic confinement is associated with the enhanced intensity of the electromagnetic field and the local density of optical states which has been exploited in fluorescence studies of single molecules[3] as well as in the measurement on ensembles of fluorophore-labeled biomolecules.[4,5] The interaction of fluorophore labels with the plasmonically enhanced electromagnetic field allows an increase of excitation rate and improvement of the collection yield of emitted fluorescence photons. The combined coupling of fluorophores at their absorption and emission wavelengths with propagating surface plasmons (PSPs) on metallic films or localized surface plasmons (LSPs) at metallic nanoparticles can be engineered to enhance detected fluorescence intensity by a factor exceeding 3 orders of magnitude.[6]

In plasmonically amplified fluorescence assays, biomolecules that are labeled with fluorophores are affinity captured on a metallic sensor surface at distances in the range of 15−20 nm at which the plasmonic fluorescence enhancement typically reaches its maximum.[7−9] At shorter distances the quenching becomes dominant and the emitted florescence signal is attenuated rather than enhanced while at longer distances the binding events occur outside the evanescent surface plasmon field. Aptamers become increasingly popular in analytical technologies for specific capture and sensitive detection of low-molecular-weight analytes[10,11] for which more commonly used antibody immunoassays are not possible. These versatile building blocks can be employed in numerous detection formats that take advantage of the measurement of fluorescence quenching,[12] plasmonic fluorescence enhancement,[13] or plasmonic near-field coupling between metallic nanoparticles.[14] Such variety of readout modality is possible through the flexibility in aptamer design that can be tailored for assays relying on conformation changes,[14] displacement,[15] or formation of sandwich[16] which are architectures not possible

to realize with conventionally used antibodies against low-molecular-weight analytes. A particularly interesting aspect of the aptamer flexibility in design is the possibility of their implementation to molecular beacon-based biosensors. In short, single-stranded nucleic acids are modified at their opposite ends with a fluorophore and a quencher and specific analyte binding is detected by changes in the fluorescence intensity. Fluorescence intensity is mediated by the aptamer analyte complex formation that leads to structural changes or most commonly displacement of complementary stem region of a hairpin aptamer, rendering the quencher and fluorophore pair to separate to a distance farther than energy transfer or quenching to occur.[17]

The majority of plasmon field-enhanced fluorescence assays that has been pursued with aptamers carrying a fluorophore attached to their DNA or RNA strand relied on chemically synthesized metallic nanoparticles that support LSPs. These modes typically confine electromagnetic energy at distances of few tens of nanometers and they have been used in fluorescence displacement assays that employ the distance-modulated plasmonic enhancement[18] of fluorescence signal or quenching.[19] In these works, the difference in the fluorescence signal from the aptamer with and without analyte captured was typically <6-fold. An aptamer fluorescence assay that is mediated by PSPs on metallic films has been reported to offer higher, 18-fold change, of fluorescence intensity upon analyte binding[20] when probed with less confined PSP field reaching about 100 nm from the metal surface.

This paper reports on the reversible direct detection of a small molecule analyte by conformational changes of a hairpin aptamer which is labeled with a fluorophore and attached to a metallic film supporting PSP modes. Plasmonic amplification of the fluorescence signal enabled in situ continuous monitoring of variations in concentration of low-molecular-weight analytes—adenosine and adenosine triphosphate. By using simulations and experiments, the rational design of the aptamer molecular spacers and optical readout is investigated based on the emitted fluorescence intensity dependence on distance, orientation of the emitter, and angular range used for the collection of the fluorescence light.

■ EXPERIMENTAL SECTION

Materials. Sodium chloride, tris hydrochloride, 4-(2-hydroxyethyl)-piperazine-1-ethanesulfonic acid (HEPES), polyethylene glycol sorbitan monolaurate (Tween 20), magnesium chloride hexahydrate, adenosine, guanosine, adenosine 5′-triphosphate (ATP) disodium salt hydrate, and tris(2-carboxyethyl)phosphine hydrochloride solution (TCEP) were purchased from Sigma-Aldrich (Austria). (11-Mercaptoundecyl)triethylene glycol (PEG-thiol, SPT-0011) was obtained from SensoPath Technologies (USA). Two DNA aptamers were synthesized by Integrated DNA Technologies (IDT-DNA, Leuven, Belgium). The ATP hairpin aptamer with the short loop sequence (SLA) consisted of Alexa Fluor 647N 5′-CA CCT GGG GGA GTA TTG CGG AGG AAG GTT PEG6 CCA GGT G-SH 3′ and the long loop ATP hairpin aptamer (LLA) sequence was Alexa Fluor 647N 5′-CA CCT GGG GGA GTA TTG CGG AGG AAG GTT TTT TTT TTT TTT TTT TTT TTT TTT TTT TTT CCA GGT G TT PEG6 -SH 3′. All reagents were used as received and buffer solutions were prepared using ultrapure water (Arium Pro, Sartorius Stedim).

Preparation of the Sensor Chips. A BK7 glass substrate was coated with 2 nm Cr and 50 nm Au films by thermal vacuum evaporation (Model HHV FL400, HHV Ltd., UK). The Au surface was rinsed with ethanol, dried under a stream of air, and stored under argon atmosphere until use. LLA or SLA aptamer was dissolved at

concentration of 1 μM in 200 μL of 10 mM Tris buffer (pH= 7.4) containing 6 mM MgCl$_2$. Afterward, the aptamer was reacted with 100-fold excess TCEP (100 μM). After 4 h of incubation, the reduced ATP hairpin aptamer solution was spiked with PEG-thiol at concentration of 10 μM and the mixture was flowed over the Au surface in a closed loop system for 2 h in order to form a self-assembled monolayer (SAM).

Optical Setup. A schematic of the optical setup can be seen in Figure 1. The sensor chip with the aptamer biointerface on top was
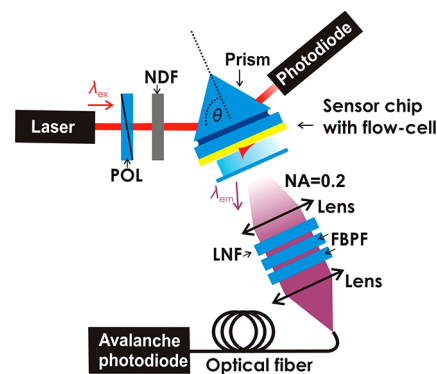

Figure 1. Schematics of the optical configuration used in the surface plasmon field-enhanced fluorescence measurements.

optically matched to an LASFN9 glass prism by using refractive index matching oil (from Cargille Inc., USA). The HeNe laser (λ_{ex} = 632.8 nm, ~2 mW) beam was transverse magnetically (TM) polarized by passing through a polarizer (POL) and was coupled to the prism to resonantly excite the PSPs by the Kretschmann configuration of the attenuated total reflection (ATR) method. The prism and sensor chip assembly was mounted on a rotation stage to control the angle of incidence θ and the angular reflectivity spectra $R(\theta)$ were measured by a photodiode detector connected to a lock-in amplifier (EG&G, USA). The enhanced field intensity occurring upon the coupling to PSPs at a resonant angle θ_{SPR} were used to excite Alexa Fluor-647 molecules at the sensor surface. The fluorescence light emitted at a wavelength around λ_{em} = 670 nm to the direction normal to the surface was collected by a lens (focal length 30 mm, numerical aperture of NA = 0.2), passed through two bandpass filters (FBF, transmission wavelength λ = 670 nm, 670FS10−25, Andover Corporation Optical Filter, USA) and a notch filter (LNF, central stop-band wavelength λ = 632.8 nm, XNF-632.8−25.0M, CVI Melles Griot, USA). Then the fluorescence light was coupled to a multimode optical fiber (FT400EMT, Thorlabs, UK) that was connected to an avalanche photodiode photon counter (Count-200-FC, Laser Components, Germany). Its intensity (F) was measured by a counter (53131A, Agilent, USA) in counts per second (cps) and recorded by the software Wasplas (Max Planck Institute for Polymer Research, Mainz, Germany). During the fluorescence measurements, the intensity of the laser beam illuminating an area of about 1 mm^2 was decreased by using a neutral-density filter (NDF, optical density OD = 2, Linos Plano Optics) in order to reduce the effect of fluorophore bleaching. The measurement of reflectivity R and fluorescence intensity F as a function of time t was performed at an incidence angle θ that was fixed close to the resonance.

Aptamer Assay. A flow-cell with a volume of 10 μL was clamped to the sensor surface to contain liquid samples transported via fluidic tubing (Tygon LMT-55) with 0.25 mm inner diameter at a flow rate of 15 μL/min. The flow-cell consisted of a PDMS gasket (thickness of ~130 μm) and a transparent glass substrate with drilled inlet and outlet ports. Throughout the assay measurements, 10 mM Tris buffer (pH = 7.4) containing 6 mM MgCl$_2$ was used (further referred to as hairpin aptamer assay buffer—HAB), which was similar to the buffer condition used during the aptamer selection process with minor modifications.[21] Following the aptamer immobilization, the sensor surface was washed for 15 min with HAB to establish a stable baseline
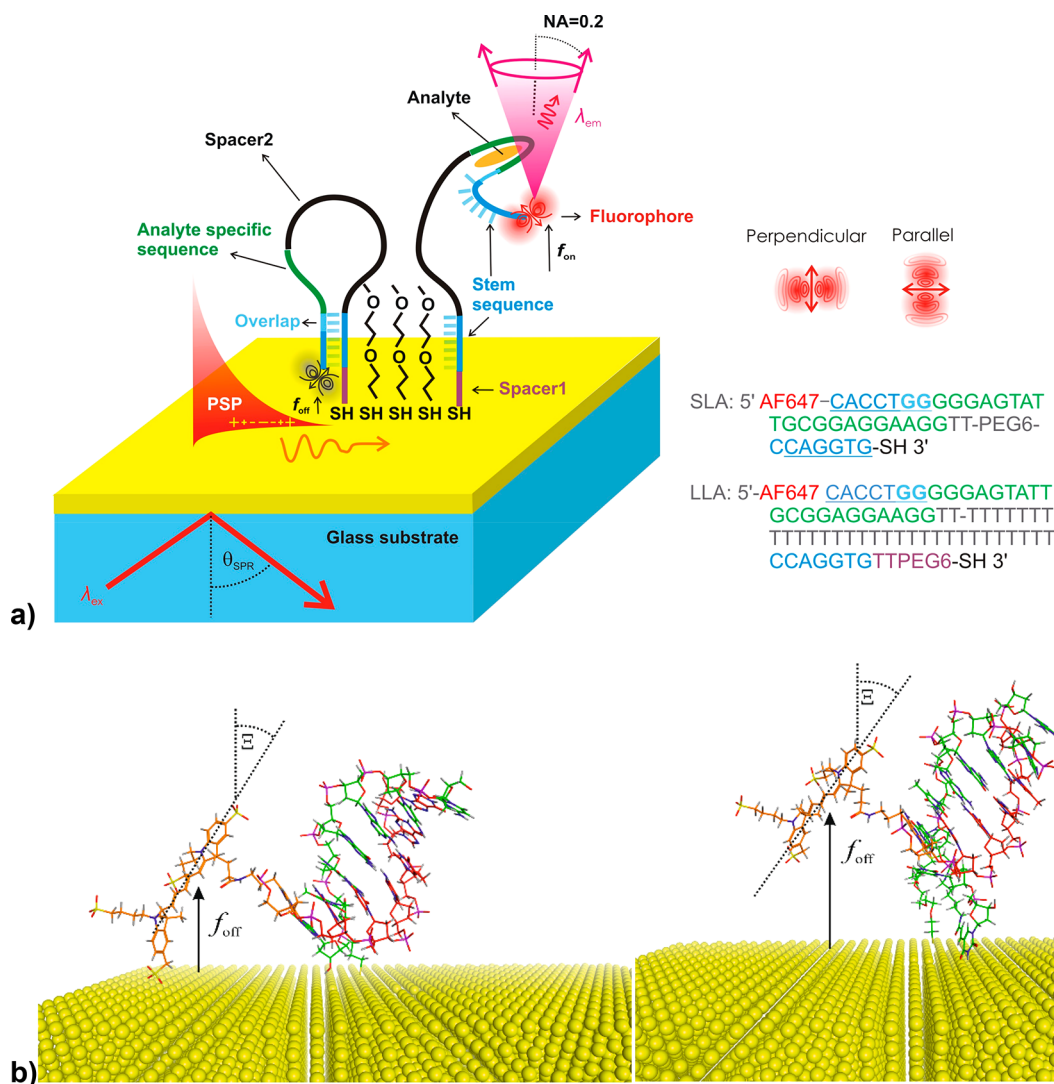
Figure 2. (a) Schematics of the aptamer-based assay on the gold sensor surface that utilizes a fluorophore coupled to surface plasmons (PSP). Short loop hairpin aptamer (SLA) or long loop hairpin aptamer (LLA) were anchored at the gold surface via a thiol group at the 3′ end and their surface density was diluted by using polyethylene glycol-thiol (PEG). (b) Examples of possible closed hairpin conformations of SLA (left) and LLA (right) in the absence of analyte and with Alexa Fluor 647 fluorophore attached to the 5′ DNA strand end.

of the fluorescence signal F_0. Then, a series of samples spiked with target and reference analytes were sequentially injected. Each sample was flowed for 3 min during which the sensor signal $F(t)$ reached saturation. For comparison, a high ionic strength HEPES buffer was used (10 mM HEPES pH = 7.4 containing 150 mM NaCl, 5 mM $MgCl_2$, and 0.005% Tween 20) for the affinity binding studies besides HAB.

Optical Simulations. Numerical simulations were carried out in order to determine the light intensity emitted to the far field by fluorophores that are exposed to the evanescent field of PSPs in close proximity to a metallic surface. The simulations were performed by using the finite difference time domain (FDTD) method that was implemented in the package FDTD Solutions (Lumerical Solutions Inc., Canada). Fluorophores were represented by an infinitely small dipole source placed above a plane gold surface at a distance f with the orientation parallel (∥) or perpendicular (⊥) to the surface. The angular distribution of emitted light intensity to the far field was determined by using a monitor placed above the structure. Perfectly matched layer boundary conditions were applied at all interfaces of a 1 μm × 1 μm × 3.5 μm simulation volume. A region of 120 nm × 120 nm × 300 nm around the emitter was studied with a 1 nm mesh, while the remaining volume was partitioned with a nonuniform conformal mesh. Water, as background medium surrounding the emitter, was

described by a constant refractive index medium with $n = 1.332$ and the wavelength-dependent refractive index of gold was obtained by fitting CRC data.[22] In order to determine the emission probability to the defined numerical aperture NA, the emitted intensity at $\lambda_{em} = 670$ nm was integrated over the angles falling in the defined range and normalized with the total emitted power at the same wavelength. The emission rate to a chosen NA was obtained as a product of emission probability and excitation rate. The excitation rate of a fluorophore was assumed proportional to the electric field intensity $|E|^2$ at $\lambda_{ex} = 633$ nm which was simulated for the resonant coupling to PSPs.

Analysis of Aptamer Conformations. A random-coil approach[23] was used based on a model in which the end-to-end distance of polymer chain with N elements is determined as $\alpha a N^{1/2}$, where a is the length between the monomers and α is a coefficient. An average distance of $a = 0.63$ nm was assumed for nucleic acid monomers[24] and $a = 0.15$ nm for the bonds within PEG segments. The segments of oligonucleotide strains were assumed to rotate completely freely and thus α was set to $\alpha = 1$. For the PEG spacers, α was set to $2^{1/2}$ to take into account their stiffer chain. It is important to note that this model neglects a wide range of effects including repulsive Coulombic interactions (e.g., between negatively charged bases in the DNA strand and with the negatively charged Alexa Fluor 647N), steric hindrance, or defined DNA strand conformations as a result of the affinity bound

target analyte. Visualizations of possible conformations of the studied aptamers were created in the Molecular Operating Environment (MOE, 2013.08, Chemical Computing Group Inc., Canada).

■ RESULTS AND DISCUSSION

As seen in Figure 2a, the gold sensor surface carried a DNA hairpin aptamer anchored via a thiol group at its 3′ end. The thiol-PEG SAM was used to dilute the surface density of the aptamer to reduce steric hindrance during analyte binding and aptamer unfolding, as well as to serve as an antifouling carpet. The aptamers specific to adenosine and adenosine triphosphate (ATP) were derived from the structure which was reported to exhibit dissociation constant in the bulk solution of $K_d \sim 6 \ \mu M$ for adenosine.[21] In order to utilize a readout strategy based on surface plasmon field-enhanced fluorescence energy transfer, the 5′ end of the aptamer strand was labeled with Alexa Fluor 647N dye. Seven bases of the aptamer at two locations close to the 5′ and 3′ ends were designed to be complementary (marked blue in Figure 2a) to form the stem. By using these sequences, the aptamer forms a hairpin structure with the fluorophore present close to the metal surface at a distance of f_{off}. The sequence of the stem region close to the 5′ end partially overlaps with the sequence of 22 bases that is specific to the target analytes adenosine and ATP (analyte specific segment marked green in Figure 2a). Therefore, the affinity binding of ATP disrupts the hairpin structure and switches the aptamer to its open conformation state with a fluorophore present at longer distance f_{on} from the gold surface. By using molecular spacers between the thiol anchor and the stem sequence (spacer 1) and between the stem sequence and the analyte specific sequence (spacer 2), the distance between Au and Alexa Fluor 647 dyes in the "off" state f_{off} and in the "on" state f_{on} can be tuned in order to achieve a maximum difference in the detected optical signals.

Distance of the Fluorophore from the Surface. Two designs of ATP aptamers with different molecular spacers 1 and 2 were used. The long loop aptamer—LLA—carried spacer 1 with 6 PEG groups and two T bases between the anchor group and the 3′ stem sequence. In addition, spacer 2 composed of 32 T bases was inserted between the ATP specific sequence and the stem sequence. The second hairpin aptamer with short loop sequence—SLA—had no spacer 1 and a shorter spacer 2 (two T bases and 6 PEG groups). To estimate the distance between the fluorophore and gold surface in the "off" and "on" states, possible conformations of the SLA and LLA were analyzed. Two examples of conformations of the stem region with the fluorophore in the closed hairpin SLA and LLA can be seen in Figure 2b. The distances of the fluorophore from the metal surface in the absence f_{off} and the presence f_{on} of the analyte were estimated based on random-coil model for polymers. For LLA with longer molecular spacers, the average distance in the closed hairpin conformation was estimated as $f_{off} \sim 1.6$ nm and in the open hairpin conformation as $f_{on} \sim 6.6$ nm. In the closed hairpin conformation, the spacer 1 (6 PEG groups and two T bases) and linker between the fluorophore and the aptamer were assumed to be flexible. Similarly, for the SLA the average distances were estimated as $f_{off} \sim 0.9$ nm and $f_{on} \sim 5.2$ nm (see summary in Table S1). The range of rotational freedom of the fluorophore dye attached to SLA and LLA in the f_{off} state is visualized in Figure S1. The Alexa Fluor 647N dye in SLA appears less flexible as compared to LLA where it possesses a broader range of possible conformational states (rotational freedom). As in the readout of the assay, the fluorescence signal

$F(t)$ is collected with about 1 s integration time, the orientation of the fluorophore is expected to be averaged and the mean polar angle is $\Xi \sim 60°$ for both "off" and "on" states when the fluorophore is free to rotate. For SLA in the closed hairpin, the fluorophore is in close proximity to the gold surface which may sterically hinder its rotation and thus a parallel orientation is likely preferred, $\Xi > 60°$ (note that a parallel orientation of the dipole corresponds to $\Xi = 90°$ and the perpendicular orientation to $\Xi = 0°$).

Simulations of Competing Plasmonic Enhancement and Quenching. The optical response of Alexa Fluor 647N to conformation changes of the investigated SLA and LLA aptamers between the closed and open hairpin states were numerically simulated by FDTD. As Figure 3a shows, PSPs
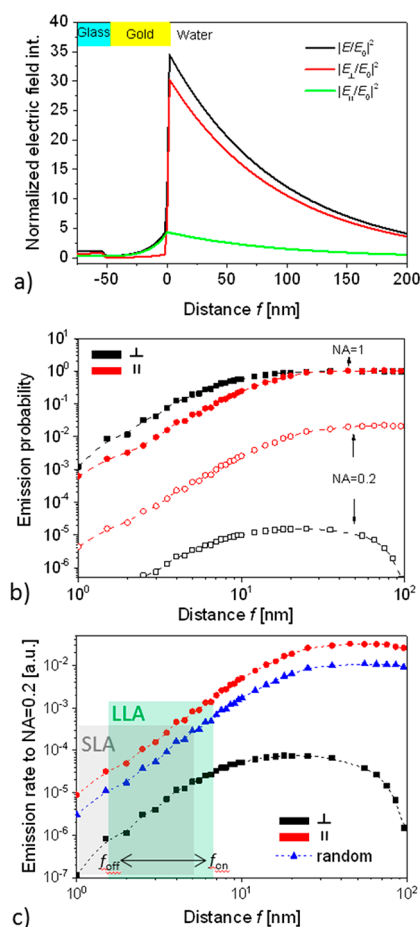
Figure 3. (a) Simulated parallel and perpendicular component of electric field intensity upon the resonant excitation of PSP at $\lambda_{ex} = 633$ nm depending on distance from the surface f. (b) Emission probability for a dipole representing the fluorophore emitting at $\lambda_{em} = 670$ nm to a cone above the gold surface with NA = 0.2 and NA = 1 as a function of distance f and dipole orientation. (c) Emission rate of a fluorophore emitting to NA = 0.2 at $\lambda_{em} = 670$ nm that is excited via PSPs at $\lambda_{ex} = 633$ nm for its parallel and perpendicular orientation and varied distance f.

probe the gold—water interface with a characteristic profile of the electromagnetic field that evanescently decays away from the gold surface with a penetration depth of about $L_p = 190$ nm (defined as the distance from the surface at which the field amplitude $|E|$ decreases by a factor of e). In addition, it shows that the field component $|E_\perp|^2$ that is perpendicular to the

surface is enhanced by a factor of about 35 with respect to that of the incident field component. The intensity of the parallel component $|E_\parallel|^2$ is approximately 5 times lower than that of the perpendicular one $|E_\perp|^2$.

In general, the radiation of fluorescence emitter placed above the plane interface between gold and water can be quenched, coupled via the near field to PSPs traveling along the gold surface, or it can be emitted to the far field. The total emission probability to the far field (represented by numerical aperture NA = 1) from a radiating dipole above the gold surface is close to 1 at long distances and it rapidly drops when decreasing the distance f below 15 nm, see Figure 3b. These data also reveal that the emitter oriented parallel ($\parallel$) to the gold emits to the far field with smaller probability than that with perpendicular orientation ($\perp$). Interestingly, this behavior is opposite if light is only collected to a narrow cone of angles close to the normal direction. The reason for the stronger emission probability from the parallel dipole (that is more quenched) into the normal direction is that emission occurs dominantly in the direction normal to dipole oscillation. Let us note that for the in situ measurement of fluorescence signal through a flow-cell, the numerical aperture NA of lens used for the collecting of fluorescence light is limited as it cannot approach close to the sensor surface. The value used herein of NA = 0.2 holds for typically used configurations in diffraction as well as ATR-based plasmon field-enhanced fluorescence biosensors.[25]

Figure 3c presents the emission rate of fluorophore that is coupled by the resonantly excited PSPs waves at wavelength λ_{ex} which occurs in a narrow angular range within NA = 0.2. It shows that the difference between the emission probability from parallel ($\parallel$) and perpendicularly ($\perp$) oriented emitter is partially compensated by the stronger excitation of perpendicular dipoles (see $|E_\perp|^2$ in Figure 3a) than parallel dipoles (see $|E_\parallel|^2$ in Figure 3a). For short distances ($1 < f < 15$ nm), the emission rate rapidly increases with increasing distance similar to the emission probability as the PSP field decays slowly. However, when increasing the distance f toward the PSP penetration depth, the emission rate decreases with the distance as the excitation field gets substantially weaker. In summary, simulations predict that fluorescence intensity detected from a fluorophore that is placed at the distance $f < 15$ nm and excited with enhanced PSP field is more than an order of magnitude stronger for the parallel dipole orientation ($\parallel$) than for the perpendicular orientation ($\perp$). The emitted fluorescence intensity rapidly increases with the distance f. For the estimated changes in the distance of randomly oriented emitter attached to LLA, the simulated intensity increase for the distance switch from $f_{off} = 1.6$ nm to $f_{on} = 6.6$ nm is a factor of about 45. For the SLA aptamer with preferably parallel oriented dye in the closed hairpin conformation, slightly lower fluorescence signal change of about 40 is predicted when the distance changes from $f_{off} = 0.9$ nm to $f_{on} = 5.2$ nm.

Measurement of Plasmon Field-Enhanced Fluorescence Energy Transfer Aptamer Assay. As seen in Figure 4a, the resonant excitation of PSPs at λ_{ex} manifests itself as a narrow resonant dip in the reflectivity spectrum $R(\theta)$. Interestingly, the measured reflectivity spectra did not show significant shift of the SPR dip located at θ_{SPR} upon the binding of ATP which increases refractive index on the surface and also leads to its redistribution due to the conformation change of the aptamer. The lack of SPR signal to such variations can be ascribed to two effects. First, ATP exhibits low molecular weight (507.2 Da) which translates to weak increase in
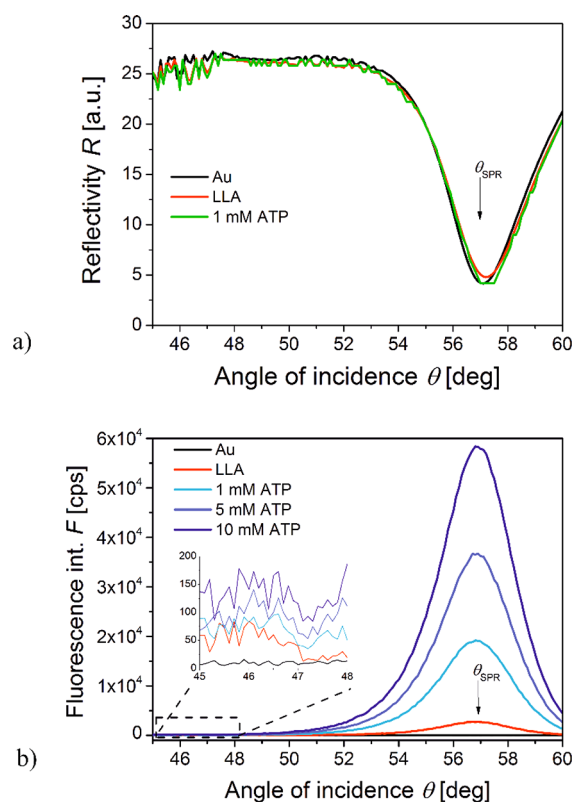

Figure 4. (a) Angular SPR reflectivity spectra $R(\theta)$ and (b) respective fluorescence intensity spectra $F(\theta)$ measured for a sensor surface in contact with HAB buffer spiked with the concentration of ATP of 0, 1, 5, and 10 mM. The gold sensor surface was functionalized with LLA.

refractive index that is proportional to $\delta\theta_{SPR}$. Second, the switching of the aptamer from its closed to open loop conformation by the capture of ATP should lead to counteracting small decrease in θ_{SPR}. Decrease of SPR angle by about $\delta\theta_{SPR} = 0.01-0.02°$ was reported for swelling of polymer brushes with molecular weight 50−3000 kDa[26] which was attributed to increase in their thickness and accompanied decrease in refractive index. The switching of the aptamer structure should lead to similar effects, but as its molecular weight of 22.6 kDa is lower, the respective SPR changes are expected to be weaker.

In the surface plasmon field-enhanced fluorescence regime, the resonant coupling to PSPs leads to the excitation of attached Alexa Fluor 647 dyes which can be seen as a strong peak in the fluorescence intensity F centered at an angle θ slightly lower than that where SPR occurs (see Figure 4b). Interestingly, the maximum fluorescence intensity occurs at angle θ that is slightly lower than that where the minimum reflectivity occurs. Such small angular shift can be attributed to the interference between the laser beam, that directly reflects from the gold layer and undergoes a phase shift and the resonantly excited surface plasmon waves that are leaky to the substrate. When incubating the sensor surface with the ATP target analyte, an increase in the fluorescence signal F is observed. This is caused by a change in the aptamer conformation that leads to an increase in the distance of the emitter from the surface f and reduced effect of quenching. Experimental measurements with SLA show 10.3-fold increase in fluorescence intensity for 12 mM ATP in comparison to the measurement taken in the absence of analyte, while for LLA, a

stronger 23.3-fold increased fluorescence intensity was observed. For the SLA, this value is about 4-fold lower than predicted and for the LLA aptamer, the measured value is about 2-fold lower than predicted. These discrepancies can be attributed to inaccuracy of the model, particularly to the simplified means of determining the distances in the open and closed hairpin conformation and approximations used in the FDTD simulations where the size of the real emitter (of about 2 nm) was replaced by an infinitely small dipole.

Real-Time Detection of the Reversible Aptamer Interaction with Target Analyte. For the experimental observation of affinity interaction with tethered aptamers, the angle of incidence was set close to $\theta_{SPR} = 57°$ (where the strongest fluorescence signal amplification occurs) and the fluorescence intensity was measured as a function of time $F(t)$. As can be seen from Figure 5, the injection of the HAB spiked
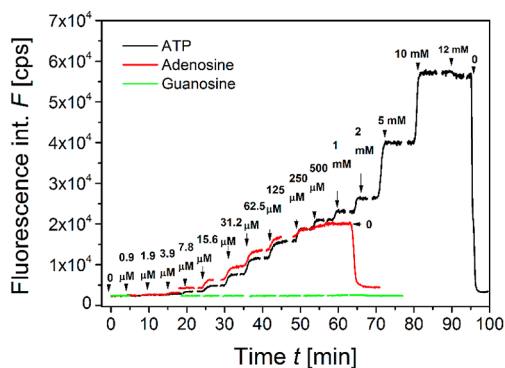

Figure 5. Example of the fluorescence signal $F(t)$ measured at a fixed angle $\theta = 57°$ during titration of ATP, adenosine, and guanosine at concentration increments up to 12 mM in HAB buffer. Gold sensor surface was functionalized with LLA.

with ATP leads to a rapid increase in the fluorescence signal F. Increasing the ATP concentration from 0.9 μM to 12 mM leads to a gradual increase in equilibrium signal F. Exposure to the highest concentration followed by rinsing in buffer (without the analyte) resulted in a rapid dissociation of the ATP-aptamer complex that manifests itself as a drop of the fluorescence signal to the original baseline value F_0. This observation confirms a fully reversible aptamer interaction for repeated measurements without regeneration. Moreover, virtually no bleaching of attached dyes was observed over the time course of the experiment. The aptamer assay showed a comparable reversible response for the detection of adenosine, but no observable response was recorded for the negative control—guanosine—which is a structural analogue of adenosine. The data for the long LLA ligand shown in Figure 5 were similar for the SLA (Figure S2).

Calibration Curves. From the data of the titration measurements, the equilibrium response F was obtained for each analyte concentration. The limit of detection (LOD) was determined as the concentration at which the calibration curve intersects with the value of the background signal F_0 plus 3 times the standard deviation, $3\sigma(F_0)$.

For SLA, the determined LOD for ATP was 108 μM and 24 μM for adenosine. This was greatly improved by the LLA where LOD values were ~1–2 μM for both ATP and adenosine. The obtained detection limits of the sensor is within the reported values in the literature, that ranges over several orders of magnitude (ATP detection limits from 0.5

pM[27] up to 0.65 mM[28]) for a plethora of fluorescence detection schemes.[29,30] Although our reported sensor may fall in the low sensitivity range, it is comparable to surface supported real-time detection sensors[31,32] and has the added value of effortless reversible detection. As can be seen in Figure 6a, the baseline
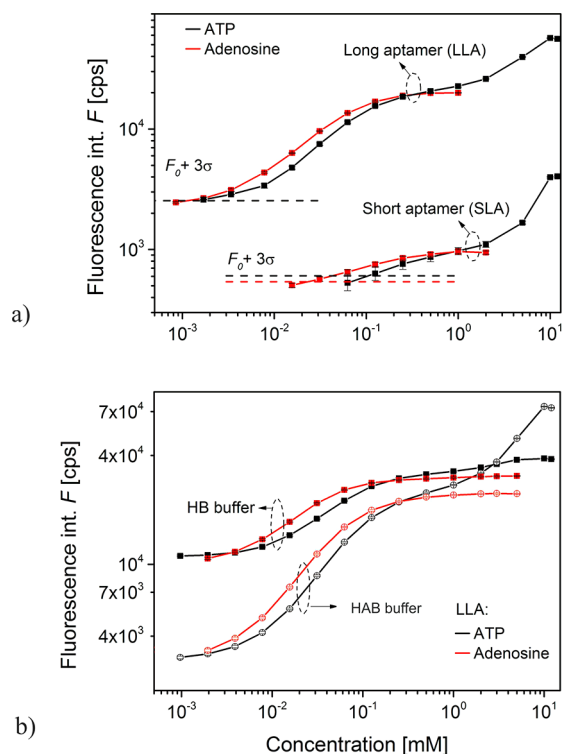

Figure 6. Calibration curves measured with SPFS detection principle for ATP and adenosine analytes. Each data points (ΔF) derived from triplicate titration measurements (an example shown in Figure 4). (a) Comparison of the response for LLA and SLA aptamers and analyte dissolved in HAB buffer. (b) Comparison of the response for LLA aptamer and analytes dissolved in HAB and HB buffers.

fluorescence intensity is higher for the interface with LLA compared to that for SLA. This can be attributed to its longer distance in the "off" aptamer state—f_{off}—(see Table S1) which is accompanied by higher emission rate (see Figure 3c). In addition, K_d values were determined from the calibration curves fitted with Langmuir isotherm model (presented in the Supporting Information) and the K_d for adenosine was of 90 μM for SLA and of 50 μM for LLA (Figures S3a,b). The calibration curves for ATP in both aptamers deviated from the Langmuir isotherm (Figure 6a). However, fitting the calibration curve for ATP concentrations up to 2 mM, where initial slight saturation was seen (Figure 5a), yields K_d values of 300 μM and 120 μM for SLA and LLA (Figure S3c,d), respectively. These values are probably increased by either the interaction of the strongly negatively charged molecule ATP with the surface-anchored aptamer that carries also negatively charged fluorophore, possibly affecting its orientation. It is worth of noting that the overall reduced affinity of fluorophore labeled aptamers with respect to the unmodified one was reported previously.[33,34] Besides the molecular charge mentioned above, surface and label induced reduction in affinity of the aptamer, the competition of target-induced conformational change from the initial closed hairpin state is a likely contributor.

It was reported that the ATP binding aptamer can be described using a "conformational selection" recognition of ATP where the analyte-free state is more stable in high salt concentration, which leads to a deteriorated distinction of conformational changes when ATP is bound.[35] Therefore, the assay buffer (HAB) used in this study did not contain NaCl, in order to increase the contrast between aptamer conformations in analyte-free/hydrizided and analyte bound states. However, it is important to observe the performance of the assay in buffers with compositions similar to samples relevant to applications in the field of medical diagnostics. For this purpose, HEPES buffer (HB) with salt concentration close to physiological conditions was used to evaluate LLA. Fluorescence intensity changes resulting from increasing analyte concentrations, in both HAB and HB, for both ATP and adenosine analytes can be seen in Figure 6b. The baseline fluorescence intensity F_0 of the sensor with HB is around 4-fold higher ($F_{0\ HB} \approx 11 \times 10^3$ cps and $F_{0\ HAB} \approx 3 \times 10^3$ cps); nevertheless the assay can be seen to perform similarly in terms of dynamic range for the detection of adenosine in both buffers. However, for ATP detection, saturation of sensor response is reached earlier in HB at 2 mM ATP, which is in contrast to 12 mM ATP for HAB and the peak intensity in HB is lower than for HAB. This decreased signal to background ratio and higher F_0 can be attributed to the influence of high salt concentration in HB, that leads to an analyte-free folded aptamer conformation and consequently lower structural change in the ATP bound state.

CONCLUSIONS

A DNA aptamer sequence specific to ATP was utilized in a plasmon field-enhanced reversible assay based on fluorescence energy transfer. The presented work demonstrates that the reversible interaction of a fluorophore-labeled aptamer with low-molecular-weight target analytes—adenosine and ATP—can be sensitively monitored in real time by plasmon field-enhanced fluorescence light intensity. The optical simulations qualitatively agree with the measured dependence of fluorescence light intensity on conformational changes of the used aptamers and they allowed ascribing the observed effects to variations in the fluorophore orientation and distance from the surface controlled by the molecular spacers. The plasmon field-enhanced fluorescence is shown to offer the advantage of continuous probing of aptamer capturing the target analyte for more than 1 h without bleaching of the dye, with a limit of detection of 1 μM. The observed design rules may provide leads to prepare more sensitive and robust assays that take advantage of versatile aptamer recognition elements and coupling with the confined field of surface plasmons in various optical configurations.

ASSOCIATED CONTENT

Ⓢ Supporting Information

The Supporting Information is available free of charge on the ACS Publications website at DOI: 10.1021/acssensors.7b00131.

> Summary of estimated distances between fluorophore and metallic surface for open and closed aptamer conformations, figures depicting the dihedral angle scan for SLA and LLA, fluorescence signal kinetics upon SLA interaction with ATP and adenosine, and fitting of calibration curves with Langmuir isotherm model in

order to determine equilibrium dissociation constant (PDF)

AUTHOR INFORMATION

Corresponding Author
*E-mail: jakub.dostalek@ait.ac.at.

ORCID ⊕
Chris Oostenbrink: 0000-0002-4232-2556
Bo Liedberg: 0000-0003-2883-6953
Jakub Dostálek: 0000-0002-0431-2170

Notes
The authors declare no competing financial interest.

REFERENCES

(1) Bauch, M.; Toma, K.; Toma, M.; Zhang, Q.; Dostalek, J. Plasmon-Enhanced Fluorescence Biosensors: a Review. *Plasmonics* **2014**, *9* (4), 781−799.

(2) Lakowicz, J. R.; Ray, K.; Chowdhury, M.; Szmacinski, H.; Fu, Y.; Zhang, J.; Nowaczyk, K. Plasmon-Controlled Fluorescence: A New Paradigm in Fluorescence Spectroscopy. *Analyst* **2008**, *133* (10), 1308−1346.

(3) Khatua, S.; Paulo, P. M. R.; Yuan, H.; Gupta, A.; Zijlstra, P.; Orrit, M. Resonant Plasmonic Enhancement of Single-Molecule Fluorescence by Individual Gold Nanorods. *ACS Nano* **2014**, *8* (5), 4440−4449.

(4) Attridge, J. W.; Daniels, P. B.; Deacon, J. K.; Robinson, G. A.; Davidson, G. P. Sensitivity Enhancement of Optical Immunosensors by the Use of a Surface Plasmon Resonance Fluoroimmunoassay. *Biosens. Bioelectron.* **1991**, *6* (3), 201−214.

(5) Liebermann, T.; Knoll, W. Surface-Plasmon Field-Enhanced Fluorescence Spectroscopy. *Colloids Surf., A* **2000**, *171* (1−3), 115−130.

(6) Kinkhabwala, A.; Yu, Z.; Fan, S.; Avlasevich, Y.; Mullen, K.; Moerner, W. E. Large Single-Molecule Fluorescence Enhancements Produced by a Bowtie Nanoantenna. *Nat. Photonics* **2009**, *3* (11), 654−657.

(7) Anger, P.; Bharadwaj, P.; Novotny, L. Enhancement and Quenching of Single-Molecule Fluorescence. *Phys. Rev. Lett.* **2006**, *96* (11), 4.

(8) Bharadwaj, P.; Novotny, L. Spectral Dependence of Single Molecule Fluorescence Enhancement. *Opt. Express* **2007**, *15* (21), 14266−14274.

(9) Vasilev, K.; Knoll, W.; Kreiter, M. Fluorescence Intensities of Chromophores in Front of a Thin Metal Film. *J. Chem. Phys.* **2004**, *120* (7), 3439−3445.

(10) Wang, R. E.; Zhang, Y.; Cai, J.; Cai, W.; Gao, T. Aptamer-Based Fluorescent Biosensors. *Curr. Med. Chem.* **2011**, *18* (27), 4175−4184.

(11) Zhou, W.; Jimmy Huang, P.-J.; Ding, J.; Liu, J. Aptamer-Based Biosensors for Biomedical Diagnostics. *Analyst* **2014**, *139* (11), 2627−2640.

(12) Zhang, J.; Wang, L.; Zhang, H.; Boey, F.; Song, S.; Fan, C. Aptamer-Based Multicolor Fluorescent Gold Nanoprobes for Multiplex Detection in Homogeneous Solution. *Small* **2010**, *6* (2), 201−204.

(13) Wood, A. J.; Basuray, S.; Bok, S.; Gangopadhyay, K.; Gangopadhyay, S.; Grant, S. A. Enhanced DNA Detection Through

the Incorporation of Nanocones and Cavities Into a Plasmonic Grating Sensor Platform. *IEEE Sens. J.* **2016**, *16* (10), 3403–3408.

(14) Lee, S. E.; Chen, Q.; Bhat, R.; Petkiewicz, S.; Smith, J. M.; Ferry, V. E.; Correia, A. L.; Alivisatos, A. P.; Bissell, M. J. Reversible Aptamer-Au Plasmon Rulers for Secreted Single Molecules. *Nano Lett.* **2015**, *15* (7), 4564–4570.

(15) Wang, W.; Chen, C.; Qian, M.; Zhao, X. S. Aptamer biosensor for protein detection using gold nanoparticles. *Anal. Biochem.* **2008**, *373* (2), 213–219.

(16) Melaine, F.; Roupioz, Y.; Buhot, A. Gold Nanoparticles Surface Plasmon Resonance Enhanced Signal for the Detection of Small Molecules on Split-Aptamer Microarrays (Small Molecules Detection from Split-Aptamers). *Microarrays* **2015**, *4* (1), 41.

(17) Wu, C.; Yang, C. J.; Tan, W. Molecular Aptamer Beacons. In *Molecular Beacons*, Yang, C. J.; Tan, W., Eds.; Springer: Berlin, Heidelberg, 2013; pp 175–194.

(18) Sui, N.; Wang, L. N.; Xie, F. X.; Liu, F. Y.; Xiao, H. L.; Liu, M. H.; Yu, W. W. Ultrasensitive Aptamer-Based Thrombin Assay Based on Metal Enhanced Fluorescence Resonance Energy Transfer. *Microchim. Acta* **2016**, *183* (5), 1563–1570.

(19) Meng, C.; Dai, Z.; Guo, W. J.; Chu, Y. Y.; Chen, G. P. Selective and Sensitive Fluorescence Aptamer Biosensors of Adenosine Triphosphate. *Nanomater. Nanotechnol.* **2016**, *6*, 33.

(20) Xie, T. T.; Liu, Q.; Cai, W. P.; Chen, Z.; Li, Y. Q. Surface Plasmon-Coupled Directional Emission Based on a Conformational-Switching Signaling Aptamer. *Chem. Commun.* **2009**, *22*, 3190–3192.

(21) Huizenga, D. E.; Szostak, J. W. A DNA Aptamer That Binds Adenosine and ATP. *Biochemistry* **1995**, *34* (2), 656–665.

(22) Williams, M. L. CRC Handbook of Chemistry and Physics. *Occup. Environ. Med.* **1996**, *53* (7), 504.

(23) Flory, P. J.; Volkenstein, M. Statistical Mechanics of Chain Molecules. *Biopolymers* **1969**, *8* (5), 699–700.

(24) Murphy, M. C.; Rasnik, I.; Cheng, W.; Lohman, T. M.; Ha, T. Probing Single-Stranded DNA Conformational Flexibility Using Fluorescence Spectroscopy. *Biophys. J.* **2004**, *86* (4), 2530–2537.

(25) Hageneder, S.; Bauch, M.; Dostalek, J. Plasmonically Amplified Bioassay − Total Internal Reflection Fluorescence vs. Epifluorescence Geometry. *Talanta* **2016**, *156−157*, 225–231.

(26) Sarkar, D.; Somasundaran, P. Conformational Dynamics of Poly(acrylic acid). A Study Using Surface Plasmon Resonance Spectroscopy. *Langmuir* **2004**, *20* (11), 4657–4664.

(27) Xue, Q.; Wang, L.; Jiang, W. A Novel Label-Free Cascade Amplification Strategy based on Dumbbell Probe-Mediated Rolling Circle Amplification-Responsive G-Quadruplex Formation for Highly Sensitive and Selective Detection of NAD+ or ATP. *Chem. Commun.* **2013**, *49* (26), 2640–2642.

(28) Xu, J.; Wei, C. The Aptamer DNA-Templated Fluorescence Silver Nanoclusters: ATP Detection and Preliminary Mechanism Investigation. *Biosens. Bioelectron.* **2017**, *87*, 422–427.

(29) Ma, C.; Lin, C.; Wang, Y.; Chen, X. DNA-based ATP sensing. *TrAC, Trends Anal. Chem.* **2016**, *77*, 226–241.

(30) Perrier, S.; Bouilloud, P.; De Oliveira Coelho, G.; Henry, M.; Peyrin, E. Small Molecule Aptamer Assays based on Fluorescence Anisotropy Signal-Enhancer Oligonucleotides. *Biosens. Bioelectron.* **2016**, *82*, 155–161.

(31) Bogomolova, A.; Aldissi, M. Real-Time Aptamer Quantum Dot Fluorescent Flow Sensor. *Biosens. Bioelectron.* **2011**, *26* (10), 4099–4103.

(32) Liu, Z.; Chen, S.; Liu, B.; Wu, J.; Zhou, Y.; He, L.; Ding, J.; Liu, J. Intracellular Detection of ATP Using an Aptamer Beacon Covalently Linked to Graphene Oxide Resisting Nonspecific Probe Displacement. *Anal. Chem.* **2014**, *86* (24), 12229–12235.

(33) Cho, E. J.; Lee, J.-W.; Ellington, A. D. Applications of Aptamers as Sensors. *Annu. Rev. Anal. Chem.* **2009**, *2* (1), 241–264.

(34) Nielsen, L. J.; Olsen, L. F.; Ozalp, V. C. Aptamers Embedded in Polyacrylamide Nanoparticles: A Tool for in Vivo Metabolite Sensing. *ACS Nano* **2010**, *4* (8), 4361–4370.

(35) Xia, T.; Yuan, J.; Fang, X. Conformational Dynamics of an ATP-Binding DNA Aptamer: A Single-Molecule Study. *J. Phys. Chem. B* **2013**, *117* (48), 14994–15003.